

Electronic Supplementary Information

Single iron atoms coordinated to g-C₃N₄ on hierarchical porous N-doped carbon polyhedra as a high-performance electrocatalyst for the oxygen reduction reaction

Tingting Sun,^{‡*a} Pianpian Zhang,^{‡a} Wenxing Chen,^b Kang Wang,^a Xianzhang Fu,^a
Tianyu Zheng,^a Jianzhuang Jiang^{*a}

^aBeijing Key Laboratory for Science and Application of Functional Molecular and Crystalline Materials, Department of Chemistry, University of Science and Technology Beijing, Beijing 100083, China

^bBeijing Key Laboratory of Construction Tailorable Advanced Functional Materials and Green Applications, School of Materials Science and Engineering, Beijing Institute of Technology, Beijing 100081, China.

*Corresponding author: ttsun99@ustb.edu.cn, jianzhuang@ustb.edu.cn

[‡] These authors contributed equally to this work.

Table of Contents

1. Experiment section.....	S2-S5
2. Supplementary Figures.....	S6-S14
3. Supplementary Tables.....	S15-S17

1. Experimental section

Chemicals. Zinc nitrate hexahydrate ($\text{Zn}(\text{NO}_3)_2 \cdot 6\text{H}_2\text{O}$, 98%, Alfa Aesar), 2-methylimidazole (MeIM, 99%, Acros Organics), iron nitrate nonahydrate ($\text{Fe}(\text{NO}_3)_3 \cdot 9\text{H}_2\text{O}$,) N, N-dimethylformamide (DMF, Sinopharm Chemical), methanol (MeOH, Sinopharm Chemical), ethanol (EtOH, Sinopharm Chemical), Nafion D-521 dispersion (5% w/w in water and 1-propanol, Alfa Aesar), commercial Pt/C (20 wt% metal, Alfa Aesar), cetyltrimethylammonium chloride solution (CTAC, 25 wt% in H_2O , Aldrich), tetraethyl orthosilicate (TEOS, $\geq 99\%$, Aldrich), KOH (analytical grade, Sinopharm Chemical), sulphuric acid (H_2SO_4 , 98%, Beijing Chemical Reagents), and hydrofluoric acid (HF, 48-51%, Acros Organics) were used without any further purification. The distilled water used in all experiments was obtained through ion-exchange and filtration.

Synthesis of ZIF-8. In a typical procedure, 2.626 g of MeIM was dissolved in a DMF-MeOH-EtOH (v/v/v = 3:1:1) mixture, and the mixture was treated by ultrasonication for 30 min to form a solution. 2.238 g of $\text{Zn}(\text{NO}_3)_2 \cdot 6\text{H}_2\text{O}$ was dissolved in DMF-MeOH (v/v = 1.5:1) to generate a clear solution. Then, the above two solutions were mixed together, and stirred for 24 h at room temperature. The as-obtained precipitates were centrifuged and washed with methanol several times and dried in vacuum at 70 °C for overnight.

Synthesis of ZIF-8@mesoSiO₂. 300 mg of the synthesized ZIF-8 and 375 mg of MeIM were dispersed in 30 mL of H_2O and 20 mL of EtOH. After 10 min of ultrasonic treatment, 0.825 ml of CTAC was added and stirred for 20 min. Then, 0.6 ml TEOS was injected into the above solution and stirred for another 2 h. The product was collected by centrifugation, washed with EtOH and H_2O , and dried under a vacuum overnight. The product was named as ZIF-8@mesoSiO₂.

Synthesis of HPNCP. The powder of ZIF-8@mesoSiO₂ was placed in a tube furnace and then heated to 920 °C for 3 h with a ramp rate of 5 °C min⁻¹ under flowing Ar gas, followed by cooling to room temperature naturally. The as-obtained powders were then immersed in aqueous HF (10 wt%) for 4 h to remove the SiO₂ protective coating. After washing thoroughly with EtOH and H₂O, the as-obtained hierarchical porous N-doped carbon polyhedrons (HPNCP) were dried oven overnight at 60 °C before further use.

Synthesis of Fe-g-C₃N₄/HPNCP catalysts. (0.2-1.6 g) of Fe(NO₃)₃·9H₂O and 7 g of urea were first dissolved in 30 mL of H₂O with stirring for 1 h at room temperature. After that, 20 mg of HPNCP was dispersed in the above precursor solution and ultrasonicated for 1h, and then stirred at room temperature for 12 h. The resulting precipitate was centrifuged and washed with 10 mL of H₂O and dried in vacuum at 60 °C overnight. Then the dried powder was transferred into a ceramic boat and placed in a tube furnace. The sample was heated to 550 °C with a heating rate of 5 °C min⁻¹ and kept at 550 °C for 3h under flowing argon gas and then naturally cooled to room temperature. By varying the amount of Fe(NO₃)₃·9H₂O in the precursor, a series of samples were synthesized. These samples are simply denoted as Fe-g-C₃N₄/HPNCP-x, where x is the quantity of Fe(NO₃)₃·9H₂O in the precursor. For comparison, Fe atoms coordinated g-C₃N₄ on N-doped carbon (Fe-g-C₃N₄/NC-0.8) was also prepared by the same process as Fe-g-C₃N₄/HPNCP-0.8 catalysts but without the SiO₂ coating.

Physicochemical characterization. Powder X-ray diffraction patterns of samples were recorded using a Rigaku RU-200b X-ray powder diffractometer (XRD) with Fe K α radiation ($\lambda = 1.5406 \text{ \AA}$). TEM images were performed on a Hitachi H-800 transmission electron microscope. The high-resolution TEM (HR-TEM), high-angle annular dark-field scanning transmission electron microscopy (HAADF-STEM) images and elemental mapping were recorded on a JEOL-2100F FETEM with electron acceleration energy of 200 kV. The scanning electron microscope (SEM) was carried out by a JSM-6700F SEM. Photoemission spectroscopy experiments (XPS) were performed at the Catalysis and Surface Science End station at the BL11U beamline of National Synchrotron Radiation Laboratory (NSRL) in Hefei, China. Elemental analysis of Fe in the solid samples was detected by an Optima 7300 DV inductively coupled plasma optical emission spectrometry (ICP-OES).

XAFS measurement and analysis. XAFS spectra at the Fe K-edge was measured at

the beamline 1W1B station of the Beijing Synchrotron Radiation Facility, China. The Fe K-edge XAFS data were recorded in a fluorescence mode. Fe foil and Fe₂O₃ were used as references. All spectra were collected in ambient conditions.

The acquired EXAFS data were processed according to the standard procedures using the ATHENA module implemented in the IFEFFIT software packages. The k^3 -weighted EXAFS spectra were obtained by subtracting the post-edge background from the overall absorption and then normalizing with respect to the edge-jump step. Subsequently, k^3 -weighted $\chi(k)$ data of Fe K-edge were Fourier transformed to real (R) space using a hanning windows ($dk=1.0 \text{ \AA}^{-1}$) to separate the EXAFS contributions from different coordination shells. To obtain the quantitative structural parameters around central atoms, least-squares curve parameter fitting was performed using the ARTEMIS module of IFEFFIT software packages.

The following EXAFS equation was used:

$$\chi(k) = \sum_j \frac{N_j S_0^2 F_j(k)}{k R_j^2} \exp[-2k^2 \sigma_j^2] \exp\left[-\frac{2R_j}{\lambda(k)}\right] \sin[2k R_j + \phi_j(k)]$$

S_0^2 is the amplitude reduction factor, $F_j(k)$ is the effective curved-wave backscattering amplitude, N_j is the number of neighbors in the j^{th} atomic shell, R_j is the distance between the X-ray absorbing central atom and the atoms in the j^{th} atomic shell (backscatterer), λ is the mean free path in \AA , $\phi_j(k)$ is the phase shift (including the phase shift for each shell and the total central atom phase shift), σ_j is the Debye-Waller parameter of the j^{th} atomic shell (variation of distances around the average R_j). The functions $F_j(k)$, λ and $\phi_j(k)$ were calculated with the ab initio code FEFF8.2. The additional details for EXAFS simulations are given below.

The coordination numbers of model samples were fixed as the nominal values. The obtained S_0^2 was fixed in the subsequent fitting. While the internal atomic distances R , Debye-Waller factor σ^2 , and the edge-energy shift ΔE_0 were allowed to run freely.

Electrochemical tests. The electrochemical experiments were performed by a CHI 660E electrochemical workstation (Shanghai Chenhua Instrument Corp., China) in a three electrode cell with a catalyst covered glassy carbon rotating disk working electrode (5 mm in diameter), a Ag/AgCl (filled with 3.5 M KCl solution) reference electrode, and a graphite rod counter electrode. All the measured potentials in this

work were converted to reverse hydrogen electrode (RHE) by the following equations: $E_{\text{RHE}} = E_{\text{Ag/AgCl}} + 0.059 \text{ pH} + E_{\text{Ag/AgCl}}^0$ ($E_{\text{Ag/AgCl}}^0 = 0.197 \text{ V}$). 5 mg of the measured catalyst (i.e., Fe-g-C₃N₄/HPNCP-x, Fe-g-C₃N₄/NC, g-C₃N₄/HPNCP, HPNCP, and commercial Pt/C) was dispersed in 960 μL of a water-isopropanol solution (v/v 3:1) containing 40 μL of 5 wt% Nafion solution by ultrasonication for at least 30 min. Then a certain volume of the catalyst ink was spread on the surface of glassy carbon electrode with the nonprecious catalyst loading was 0.48 mg cm⁻² and the loading of 20 wt% Pt/C was 0.12 mg cm⁻² and then dried under room temperature. The electrochemical experiments were conducted in O₂-saturated 0.1 M KOH at room temperature. Linear sweep voltammetry was measured at a scan rate of 5 mV s⁻¹ with an electrode rotation speed of 1600 rpm. The RDE measurements were carried out under the rotation rates ranging from 400 to 2500 rpm at a scan rate of 5 mV·s⁻¹. All polarization curves were corrected for the iR contribution within the cell. Prior to the electrochemical measurement, the electrolyte was saturated with oxygen by bubbling O₂ for at least 30 min. The electron transfer numbers (n) and kinetic currents (j_k) involved in the typical ORR process were calculated on the basis of the Koutecky-Levich equation:

$$\frac{1}{j} = \frac{1}{j_k} + \frac{1}{j_d} = \frac{1}{j_k} + \frac{1}{B\omega^{1/2}}$$

$$B = 0.62nFC_0(D_0)^{2/3}\nu^{-1/6}$$

where j is the measured current density, j_k and j_d are the kinetic-limiting and diffusion-limiting current densities, ω is the angular velocity of the disk, n is the electron transfer number, F is the Faraday constant (96485 C mol⁻¹), D_0 is the diffusion coefficient of oxygen in the electrolyte ($1.9 \times 10^{-5} \text{ cm}^2 \text{ s}^{-1}$), ν is the kinetic viscosity of the electrolyte ($0.01 \text{ cm}^2 \text{ s}^{-1}$), and C_0 is the bulk concentration of oxygen ($1.2 \times 10^{-6} \text{ mol cm}^{-3}$). The accelerated degradation testing was performed by running 5000 CV cycles on the electrode between 0.2 and 1.0 V vs. RHE with a scan rate of 100 mV s⁻¹.

2. Supplementary Figures

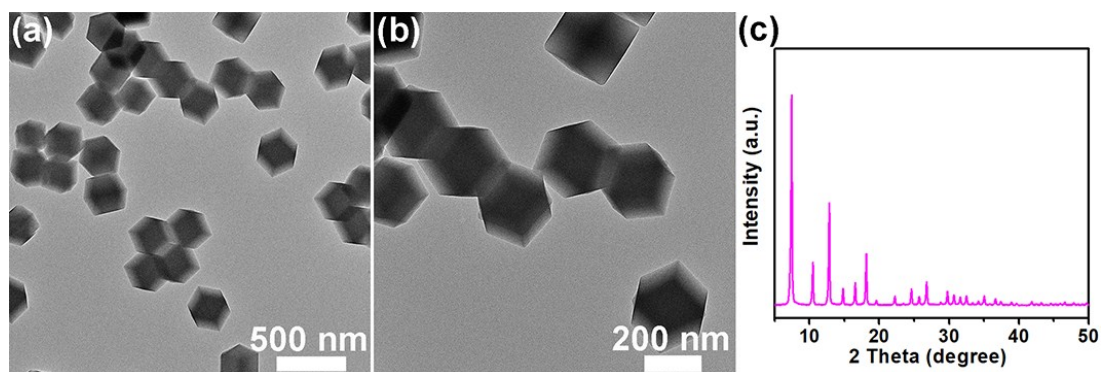


Fig. S1. (a,b) TEM images of ZIF-8 and (c) XRD pattern of ZIF-8

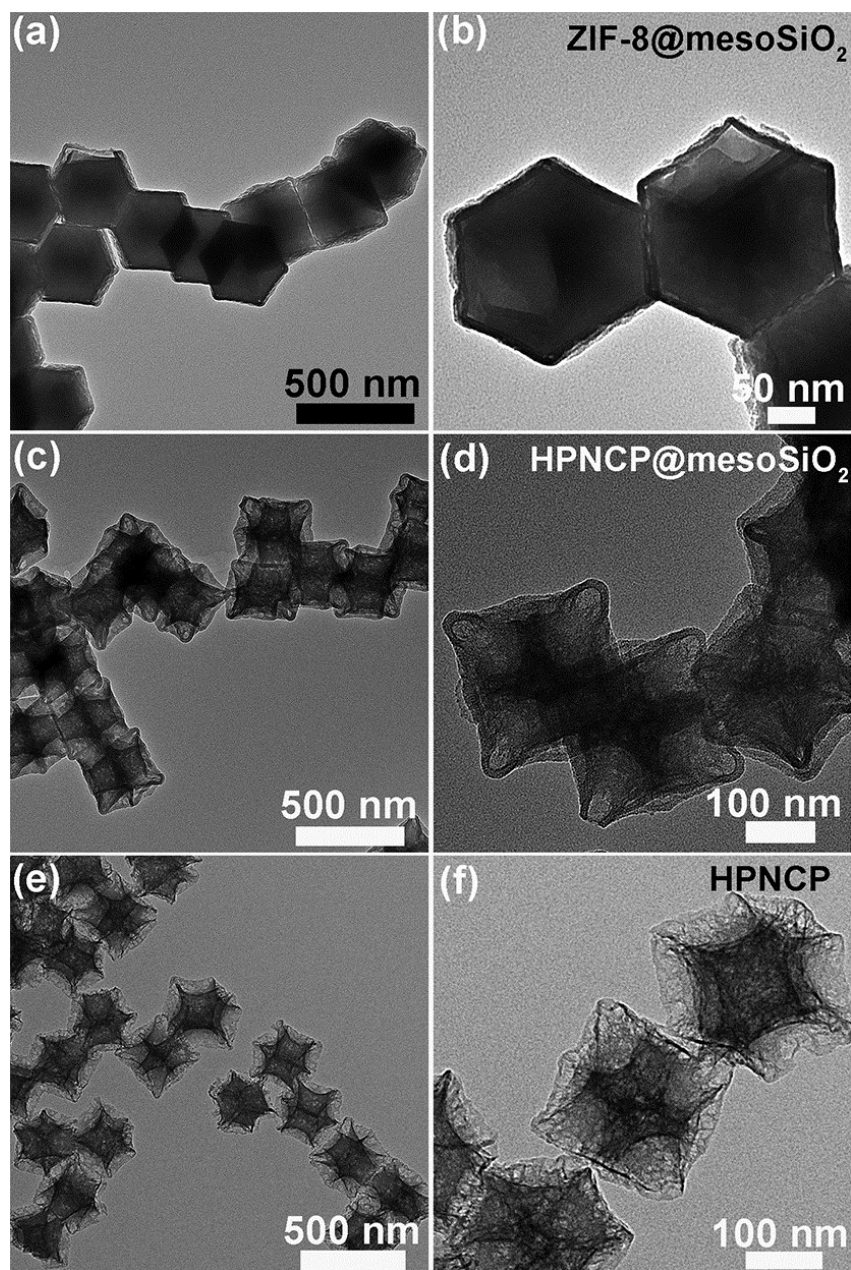


Fig. S2. TEM images of (a,b) ZIF-8@mesoSiO₂, (c,d) HPNCP@mesoSiO₂, and (e,f) HPNCP.

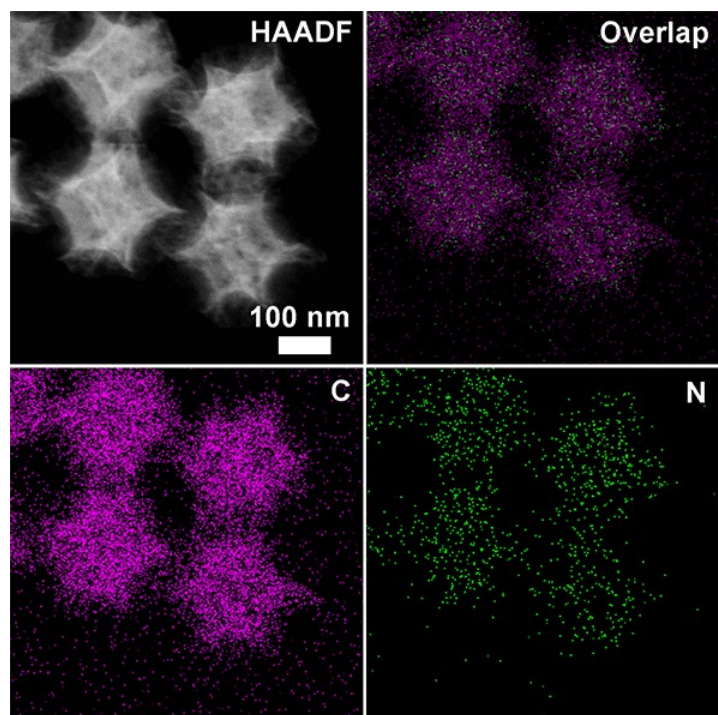


Fig. S3. HAADF-STEM image of HPNCP and corresponding element maps showing the distribution of C (purple), and N (green).

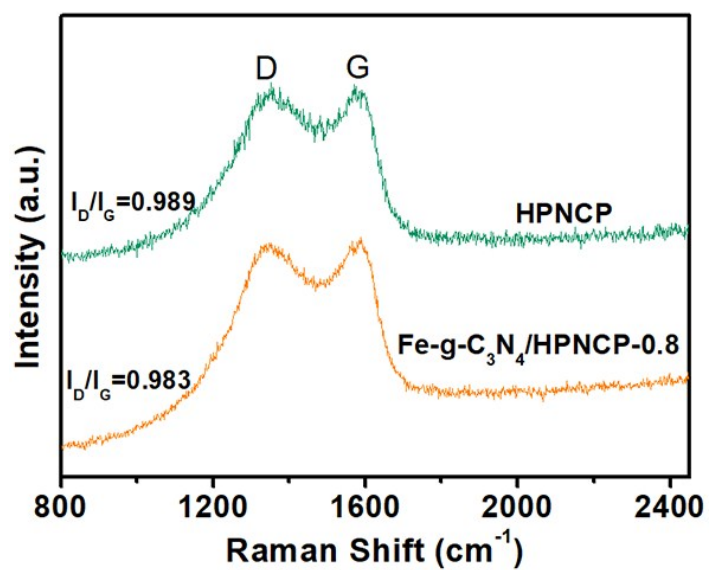


Fig. S4. Raman spectra of Fe-g-C₃N₄/HPNCP-0.8 and HPNCP.

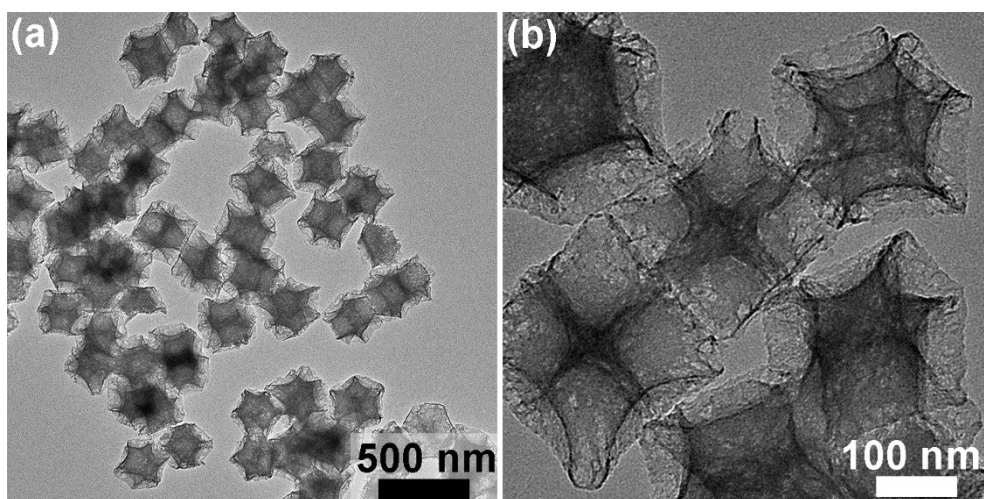


Fig. S5. (a) TEM images of g-C₃N₄/HPNCP.

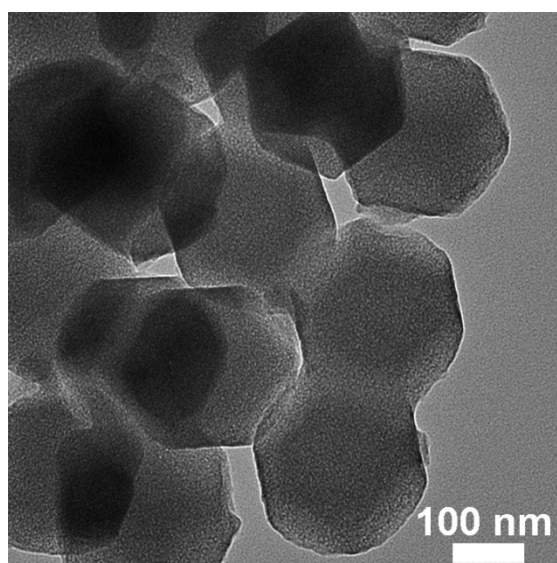


Fig. S6. TEM image of Fe-g-C₃N₄/NC-0.8. The obtained Fe-g-C₃N₄/NC-0.8 material maintains the original dodecahedral particle shape of ZIF-8.

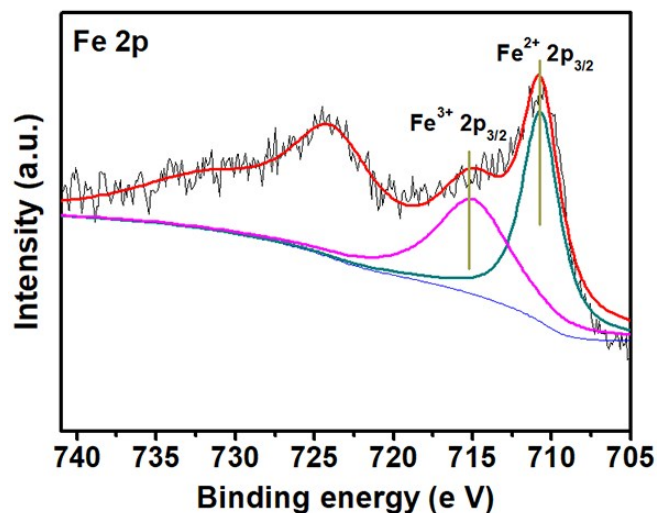


Fig. S7. The high resolution XPS spectrum of Fe 2p for the Fe-g-C₃N₄/HPNCP-0.8 sample. The Fe 2p_{3/2} peak appears at around 710.7 eV can be assigned to the N-coordinated Fe, again proving the formation of Fe-N_x configuration.

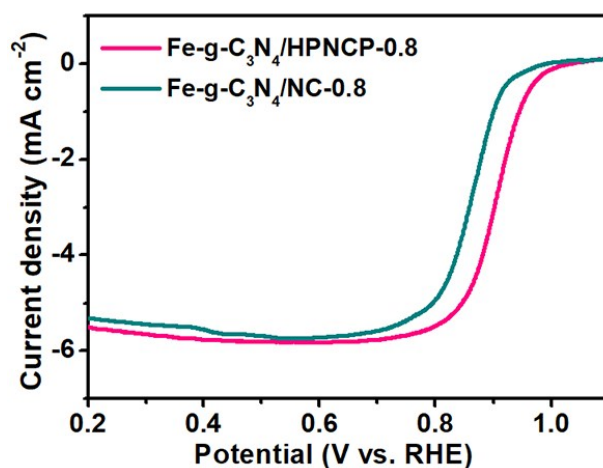


Fig. S8. ORR LSV curves of Fe-g-C₃N₄/HPNCP-0.8 and Fe-g-C₃N₄/NC-0.8.

As shown in Fig. S8, the Fe-g-C₃N₄/HPNCP-0.8 catalyst delivers enhanced ORR activity with a highly positive half-wave potential ($E_{1/2}$) of 0.902 V vs. RHE, 38 mV higher than the $E_{1/2}$ value of the Fe-g-C₃N₄/NC-0.8 catalyst (0.864 V). The enhanced ORR activity of Fe-g-C₃N₄/HPNCP-0.8 compared with Fe-g-C₃N₄/NC-0.8 is found to stem from the high utilization of Fe-N_x moieties by Fe-g-C₃N₄/HPNCP-0.8, owing to the efficient mass transport property in the additional mesopores on the wall. Such a concave nanoparticle with largely enhanced mesoporosity plays a crucial role in increasing the accessibility of Fe-N_x moieties and enhancing the mass transport of the catalyst layer during the ORR process.

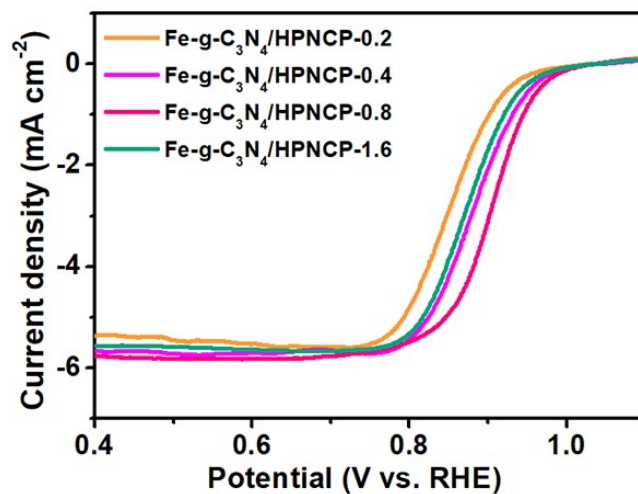


Fig. S9. ORR LSV curves of Fe-g-C₃N₄/HPNCP catalysts with different Fe contents.

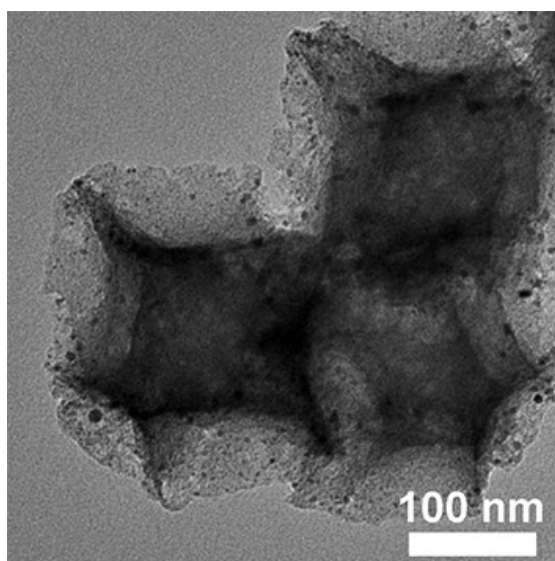


Fig. S10. TEM image of Fe-g-C₃N₄/HPNCP-1.6 sample.

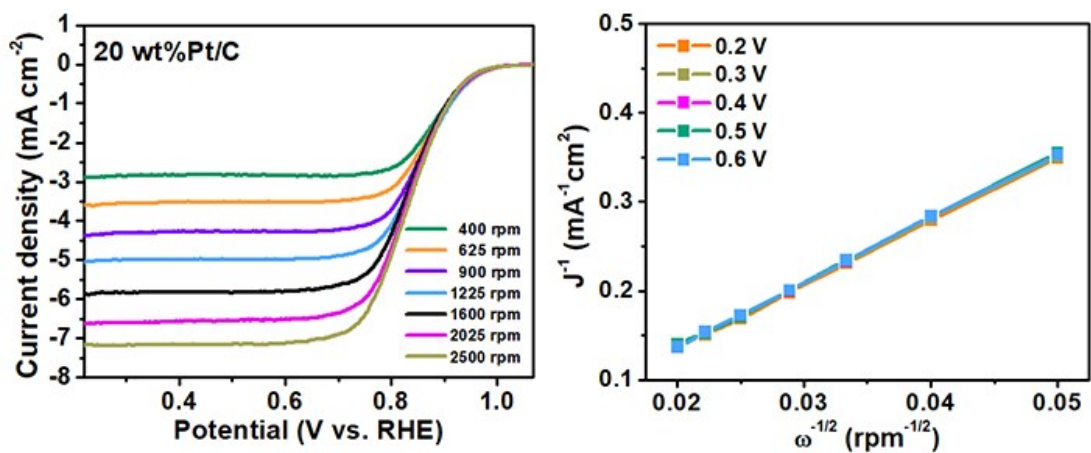


Fig. S11. LSV curves of 20 wt% Pt/C in O₂-saturated 0.1 M KOH at 400-2500 rpm and the corresponding K-L plots at various potentials.

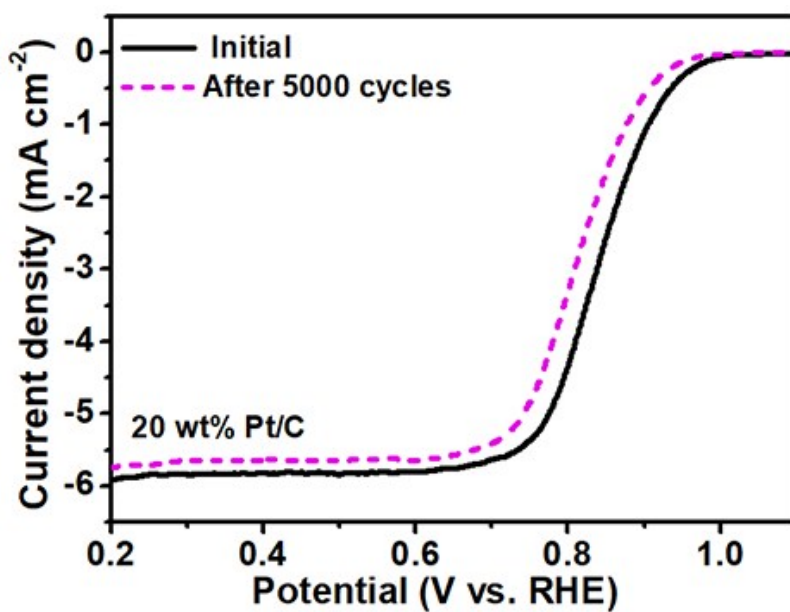


Fig. S12. ORR LSV curves of Pt/C initially and after 5000 cycles between 0.5 and 1.0 V at a scan rate 100 mV s⁻¹.

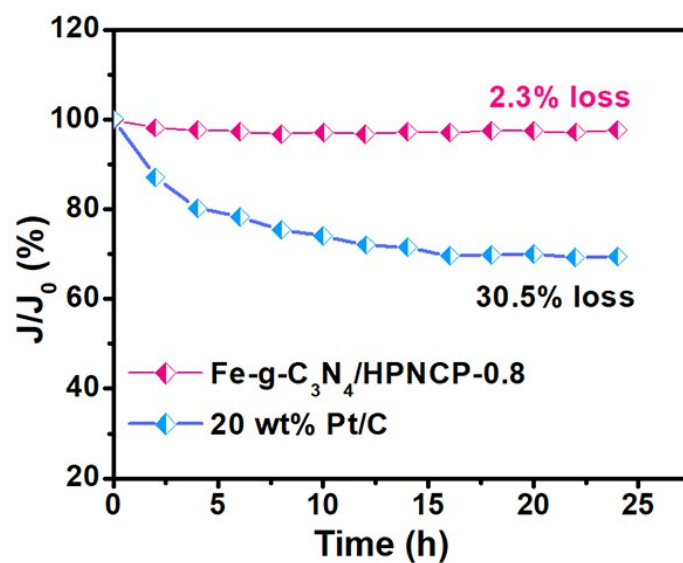


Fig. S13. Retention percentage of the catalytic current for Fe-g-C₃N₄/HPNCP-0.8 and Pt/C at the potential of 0.60 V vs. RHE.

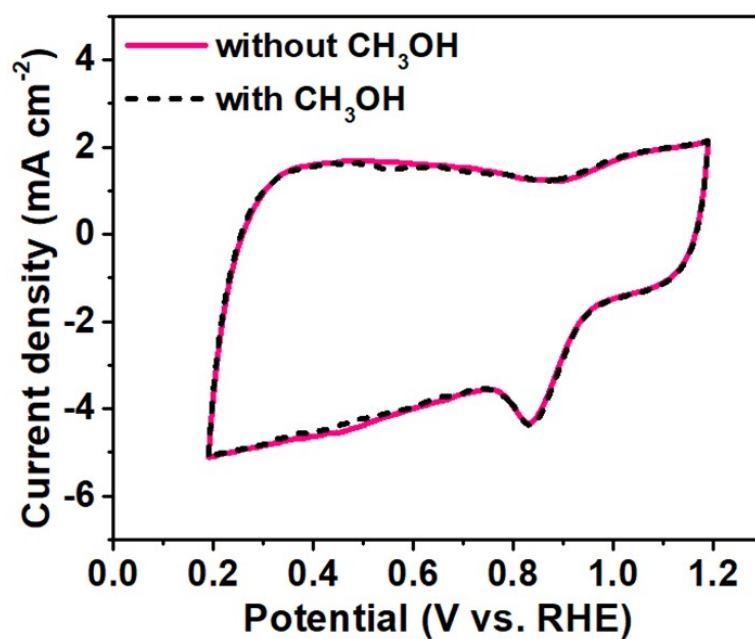


Fig. S14. CVs of Fe-g-C₃N₄/HPNCP-0.8 in O₂-saturated 0.1 M KOH without and with 1.0 M CH₃OH.

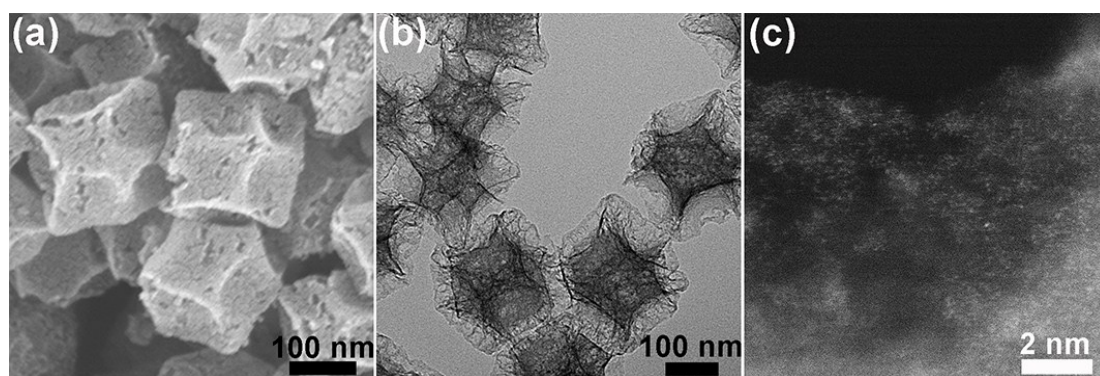


Fig. S15. (a) SEM, (b) TEM, and (c) AC HAADF-STEM images of Fe-g-C₃N₄/HPNCP-0.8 after 5000 cycles in 0.1 M KOH.

3. Supplementary Tables

Table S1. Structural parameters extracted from the Fe K-edge EXAFS fitting. ($S_0^2=0.85$)

sample	Scattering pair	CN	R(\AA)	$\sigma^2(10^{-3}\text{\AA}^2)$	$\Delta E_0(\text{eV})$	R factor
Fe-g-C ₃ N ₄ /HPNCP-0.8	Fe-N	1.9	2.00	5.2	0.5	0.005

S_0^2 is the amplitude reduction factor; CN is the coordination number; R is interatomic distance (the bond length between central atoms and surrounding coordination atoms); σ^2 is Debye-Waller factor (a measure of thermal and static disorder in absorber-scatterer distances); ΔE_0 is edge-energy shift (the difference between the zero kinetic energy value of the sample and that of the theoretical model). R factor is used to value the goodness of the fitting.

Error bounds that characterize the structural parameters obtained by EXAFS spectroscopy were estimated as $N \pm 20\%$; $R \pm 1\%$; $\sigma^2 \pm 20\%$; $\Delta E_0 \pm 20\%$.

Table S2 Comparison of the electrocatalytic ORR activity of Fe-g-C₃N₄/HPNCP-0.8 with other representative non-noble-metal ORR electrocatalysts recently reported in the literatures.

Catalyst	Electrolyte	Loading (mg cm ⁻²)	$E_{1/2}$ (V vs. RHE)	Reference
Fe-g-C ₃ N ₄ /HPNCP-0.8	0.1 M KOH	0.48	0.902	This work
m-FeSNC	0.1 M KOH	0.408	0.904	<i>Chem. Commun.</i> , 2018 , 54, 12073-12076.
Fe ₃ N-PCN	0.1 M KOH	0.6	0.870	<i>Chem. Commun.</i> , 2019 , 55, 5789-5792.
Fe NS-PC-800	0.1 M KOH	N.A.	0.85	<i>Chem. Commun.</i> , 2018 , 54, 12974-12977.
SA-Fe/NG	0.1 M KOH	0.24	0.88	<i>Proc. Natl. Acad. Sci. USA</i> 2018 , 10.1073/pnas.1800771115.
Fe-SAs/NPS-HC	0.1 M KOH	N.A.	0.912	<i>Nat. Commun.</i> 2018 , 9, 5422.
Cu-SAs/N-C	0.1 M KOH	0.09	0.895	<i>Nat. Catal.</i> 2018 , 1, 781-786.
Fe SAs/N-C	0.1 M KOH	0.25	0.91	<i>ACS Catal.</i> 2019 , 9, 2158-2163.
Co-SAs@NC	0.1 M KOH	0.612	0.82	<i>Angew. Chem. Int. Ed.</i> 2019 , 58, 5359-5364.
Co SA@NCF/CNF	0.1 M KOH	0.4	0.88	<i>Adv. Mater.</i> 2019 , 1808267.
Cu-N-C	0.1 M KOH	N.A.	0.869	<i>Energy Environ. Sci.</i> , 2018 , 11, 2263-2269.
Fe/N/S-PCNT	0.1 M KOH	0.1	0.84	<i>J. Mater. Chem. A</i> , 2019 , 7, 1607-1615.

Al and N codoped graphene	0.1 M KOH	0.15	0.86	<i>ACS Catal.</i> 2019 , <i>9</i> , 610-619.
CCNTs-Co-800	0.1 M KOH	0.198	0.84	<i>Angew. Chem. Int. Ed.</i> 2018 , <i>57</i> , 13187-13191.
C-MOF-C2-900	0.1 M KOH	N.A.	0.82	<i>Adv. Mater.</i> 2018 , <i>30</i> , 1705431.
Fe-NPC	0.1 M KOH	0.5	0.883	<i>Appl. Catal. B: Environ.</i> 2019 , <i>249</i> , 306-315.
Fe-N-C	0.1 M KOH	0.56	0.90	<i>Nano Energy</i> 2019 , <i>61</i> , 60-68.
Fe SAs-N/C-20	0.1 M KOH	0.408	0.909	<i>J. Am. Chem. Soc.</i> 2018 , <i>140</i> , 11594-11598.
Zn-N-C-1	0.1 M KOH	0.08	0.873	<i>Angew. Chem. Int. Ed.</i> 2019 , <i>58</i> , 7035-7039.
cal-CoZIF-VXC72-H	0.1 M KOH	0.4	0.86	<i>Adv. Mater.</i> 2017 , 1701354.
Fe@Aza-PON	0.1 M KOH	N.A.	0.839	<i>J. Am. Chem. Soc.</i> 2018 , <i>140</i> , 1737-1742.
Mn/C-NO	0.1 M KOH	0.3	0.86	<i>Adv. Mater.</i> 2018 , 1801732.
S,N-FeN/CCNT	0.1 M KOH	0.6	0.85	<i>Angew. Chem. Int. Ed.</i> 2017 , <i>56</i> , 610.
Co-N/CNFs	0.1 M KOH	0.1	0.82	<i>ACS Catal.</i> 2017 , <i>7</i> , 6864-6871.
SA-Fe-HPC	0.1 M KOH	0.1	0.89	<i>Angew. Chem. Int. Ed.</i> 2018 , <i>57</i> , 1-7.
Fe ₃ C@N-CNT	0.1 M KOH	0.25	0.85	<i>Energy Environ. Sci.</i> 2016 , <i>9</i> , 3092-3096.